

Technical Note

# Contributions of Various Sources to the Higher-Concentration Center of CO within the ASM Anticyclone Based on GEOS-Chem Simulations

Yuepeng Yang <sup>1</sup> , Qian Li <sup>2,\*</sup>, Haoyue Wang <sup>1</sup>, Zhixuan Bai <sup>2</sup>, Dan Li <sup>2</sup>, Weiguo Wang <sup>1</sup> and Jianchun Bian <sup>2,3,4</sup>

<sup>1</sup> School of Earth Sciences, Yunnan University, Kunming 650500, China; yyp@mail.ynu.edu.cn (Y.Y.); wanghaoyue22@ynu.edu.cn (H.W.); wangwg@ynu.edu.cn (W.W.)

<sup>2</sup> Key Laboratory of Middle Atmosphere and Global Environment Observation, Institute of Atmospheric Physics, Chinese Academy of Sciences, Beijing 100029, China; baizhixuan@mail.iap.ac.cn (Z.B.); lidan@mail.iap.ac.cn (D.L.); bjc@mail.iap.ac.cn (J.B.)

<sup>3</sup> College of Earth and Planetary Sciences, Chinese Academy of Sciences, Beijing 100049, China

<sup>4</sup> College of Atmospheric Sciences, Lanzhou University, Lanzhou 730000, China

\* Correspondence: qian.li@mail.iap.ac.cn; Tel.: +86-10-8299-5284

**Abstract:** Satellite observations show that carbon monoxide (CO) concentration centers exist in the tropopause region of the Tibetan Plateau, while their sources and formation mechanism still remain uncertain. In this paper, the 3-D chemical transport model GEOS-Chem is used to conduct sensitivity analysis in 2016. Combined with the analysis data and satellite data, the contribution of three important emission sources (South Asia, East Asia and Southeast Asia) and two important chemical reaction species (CH<sub>4</sub> and nonmethane volatile organic compounds (NMVOCs)) to CO in the upper troposphere and lower stratosphere (UTLS) are studied. The results show that in the Asian monsoon region CO emissions originating from the surface are transported to the upper troposphere via a deep convection process and then enter the Asian Summer Monsoon (ASM) anticyclone. The strong ASM anticyclone isolates the mixing process of air inside and outside the anticyclone, upon entry of carbon monoxide-rich air. In the lower stratosphere, the intensity of the ASM anticyclone declines and the air within the anticyclone flows southwestward with monsoon circulation. We found that in the summer Asian monsoon region, South Asia exhibited the highest carbon monoxide concentration transported to the UTLS. CH<sub>4</sub> imposed the greatest influence on the CO concentration in the UTLS region. According to the model simulation results, the CO concentrations in the Asian monsoon region at 100 hPa altitudes were higher than those in other regions at the same latitudes. Regarding effects, 43.18% originated from CH<sub>4</sub> chemical reactions, 20.81% originated from NMVOC chemical reactions, and 63.33% originated from surface CO emissions, while sinks yielded a negative contribution of −27.32%. Regarding surface CO emissions, East Asia contributed 13.56%, South Asia contributed 39.27%, and Southeast Asia contributed 7.15%.

**Keywords:** upper troposphere and lower stratosphere; carbon monoxide; South Asia high pressure; atmospheric chemical transport model



**Citation:** Yang, Y.; Li, Q.; Wang, H.; Bai, Z.; Li, D.; Wang, W.; Bian, J.

Contributions of Various Sources to the Higher-Concentration Center of CO within the ASM Anticyclone Based on GEOS-Chem Simulations. *Remote Sens.* **2022**, *14*, 3322. <https://doi.org/10.3390/rs14143322>

Academic Editor: Fei Xie

Received: 15 May 2022

Accepted: 8 July 2022

Published: 10 July 2022

**Publisher's Note:** MDPI stays neutral with regard to jurisdictional claims in published maps and institutional affiliations.



**Copyright:** © 2022 by the authors. Licensee MDPI, Basel, Switzerland. This article is an open access article distributed under the terms and conditions of the Creative Commons Attribution (CC BY) license (<https://creativecommons.org/licenses/by/4.0/>).

## 1. Introduction

Stratosphere-troposphere exchange (STE) entails the transport process of atmospheric chemical components across the tropopause [1]. STE processes notably influence the spatial distribution of atmospheric components and atmospheric circulation. For example, the Brewer–Dobson circulation is a global-scale meridional circulation in the stratosphere [2,3]. Tropospheric air can reach the stratosphere across the tropopause through the ascending branch of the Brewer–Dobson circulation, and stratospheric air can also enter the troposphere through the descending branch of the Brewer–Dobson circulation [4]. However, as the ascending branch of the Brewer–Dobson circulation mainly participates in the STE process in the tropical region, the underlying surface of the tropical region is dominated by the

ocean, and the air is relatively clean [5,6]. Therefore, the material transport and exchange process over the heavily polluted Asian monsoon region has aroused the interest of many scholars [7]. ASM anticyclone system is considered to be an important transport pathway for water vapor and pollutants into the stratosphere [8]. With a substantial amount of organic and sulfur emissions in Asia, the ASM anticyclone serves as an efficient smokestack venting aerosols to the upper troposphere and lower stratosphere [9]. Many satellite observations indicate that the location of the monsoon anticyclone in the upper troposphere and lower stratosphere (UTLS) region corresponds to the extreme center of the atmospheric composition in summer. For example, the concentration of atmospheric components in the troposphere (HCN, water vapor, CO, and CH<sub>4</sub>) in this region is significantly higher than that in other regions at the same latitudes [7,10,11].

A deep convection system is another important process of vertical transport of the atmospheric mass, which can transport air from the surface to the upper troposphere or even the lower stratosphere [12]. This process can transport trace gases in the atmosphere over a longer period of time. These trace gases typically exhibit a longer lifetime or retention time in the UTLS region than that in the lower troposphere. Therefore, the spatial distribution characteristics and content of these trace gases in the upper troposphere or lower stratosphere are closely related to the deep convective system [13]. Deep convective processes transport air in the lower troposphere to the UTLS region [14]. Scholars used the Model for Ozone and Related Tracers 4 (MOZART 4) to simulate the source of CO in ASM anticyclones in the UTLS region and found that CO mainly stemmed from India and Southeast Asia [15]. In addition to the above two areas, eastern China is a high-CO emission area [16,17]. The monsoon circulation in East Asia is different from that in South Asia. Regarding the STE process, the intensity of the plum rain period in East Asia can affect the transport of pollutants in the upper air [18].

In the next section, we describe the numerical models, satellite data and reanalysis data applied in this study. In Section 3, we analyze the dynamic process of air transport from the lower troposphere to the UTLS region and quantify the effects of surface emissions and chemistry on high-altitude CO concentrations. Finally, the main conclusions of this study are outlined in the fourth section.

## 2. Data and Methods

### 2.1. Model Description and Experimental Setup

GEOS-Chem is a global 3-D model of the atmospheric chemistry driven by meteorological inputs retrieved from the Goddard Earth Observation System (GEOS) of the NASA Global Modeling and Assimilation Office. We used version 12.9.3 (<http://acmg.seas.harvard.edu/geos/>), driven by Modern-Era Retrospective analysis for Research and Applications (MERRA-2) reanalysis data. The model was applied to simulate CO globally in the 2° × 2.5° GEOS-Chem horizontal grid. Tagged-CO is a calculation scheme of the GEOS-Chem model, and only the CO concentration and distribution were simulated. Compared to the full chemical simulation scheme, the chosen scheme could save more computing time. All the relevant simulation experiments adopted in this paper are tagged-CO experiments. CO concentrations were calculated based on surface emissions and chemical effects by using different carbon monoxide emission inventories for different areas. Anthropogenic emissions in Canada were retrieved from the Air Pollutant Emission Inventory (APEI) v2016. The National Emission Inventory (NEI) v2015-03 was used for North American regional emissions. The Diffuse and Inefficient Combustion Emissions in Africa (DICE-Africa) inventory includes anthropogenic emissions originating from biofuel burning and fossil fuel burning in the African region [19]. MIX v1.1 listings were used for Asia [20]. Emissions stemming from aircraft and ships worldwide are contained in the Community Emissions Data System (CEDS) inventory [21]. The Global Fire Emissions Database (GFED2) inventory provided data on carbon monoxide emissions stemming from biomass burning. The volatile organic compound (VOC) biological source emission inventory was calculated via the Model of Emissions of Gases and Aerosols from Nature (MEGAN) [22].

Combined with the above inventory, Figure 1a shows the five-year average results of summer surface emission rates from 2016–2020. Regions with  $OLR \leq 220 \text{ W/m}^2$  were used to represent areas with a high incidence of deep convective activity [23]. Figure 1b show Five-year average results of surface emission OLR in summer (June, July and August) from 2016–2020. The white area indicates the area of  $OLR \leq 220 \text{ W/m}^2$ . In the simulation, the time step of convection transport and parallel transport are 10 min. Regarding the chemical processes involved in the GEOS-Chem model, the simulations were performed at a time step of 20 min.

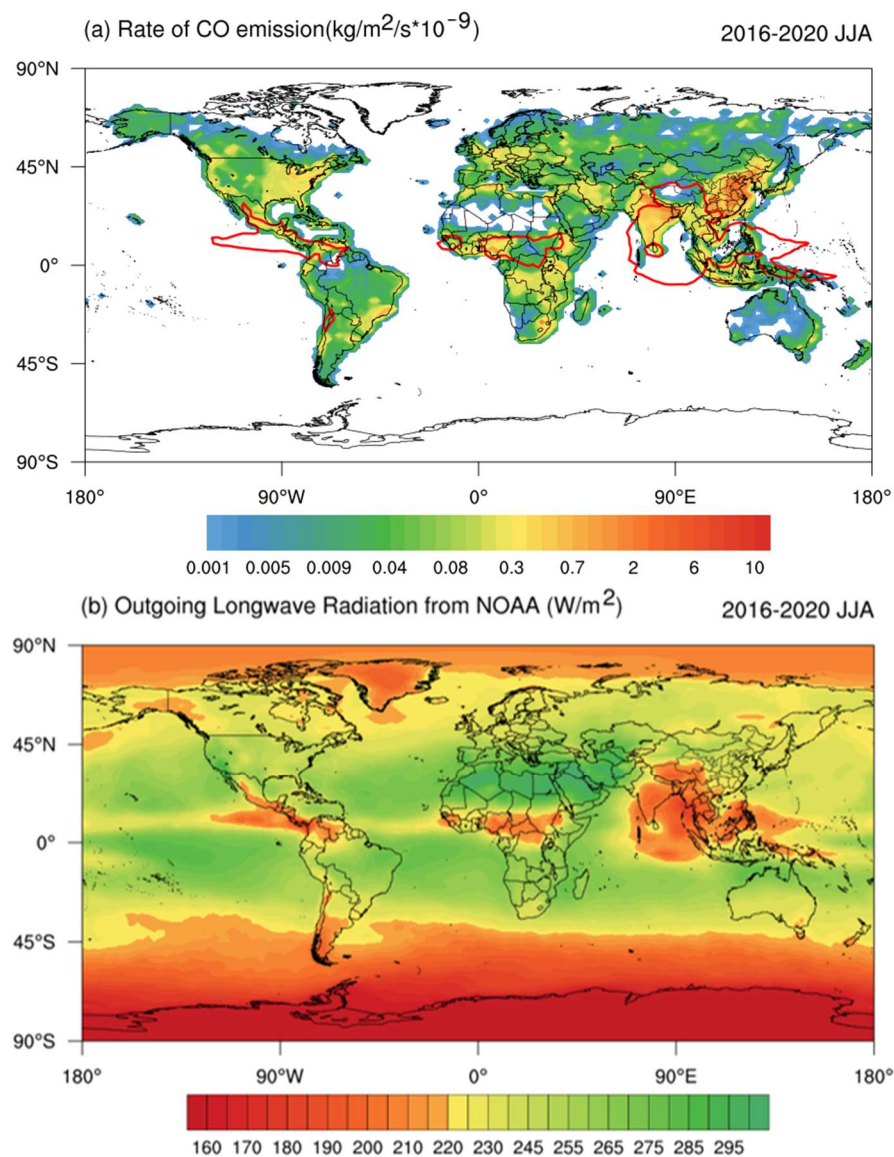


**Figure 1.** Five-year average results of surface emission rate (a) and OLR (b) in summer (June, July and August) from 2016–2020. The red line represents the area where  $OLR \leq 220 \text{ W/m}^2$ .

Global CO concentrations were simulated at altitudes ranging from the surface to 0.01 hPa. The three regions shown in Figure 2 have relatively high surface CO emissions in Asia. We focused on the contribution of surface CO emissions in these three regions to the CO concentration in the UTLS over the Tibetan Plateau. As shown in Figure 2, parts of eastern China and surrounding countries belong to East Asia. Among these parts, Xinjiang and Tibet in China were not included in this study because their surface emission sources were relatively negligible. The Philippines, Laos, Thailand, Vietnam, Cambodia, Myanmar, Malaysia, Brunei, Singapore, Indonesia, Timor-Leste and Papua New Guinea and their

surrounding waters were designated as Southeast Asia. India, Bangladesh, Nepal, Sri Lanka, Bhutan and Pakistan and their surrounding waters were defined as South Asia.

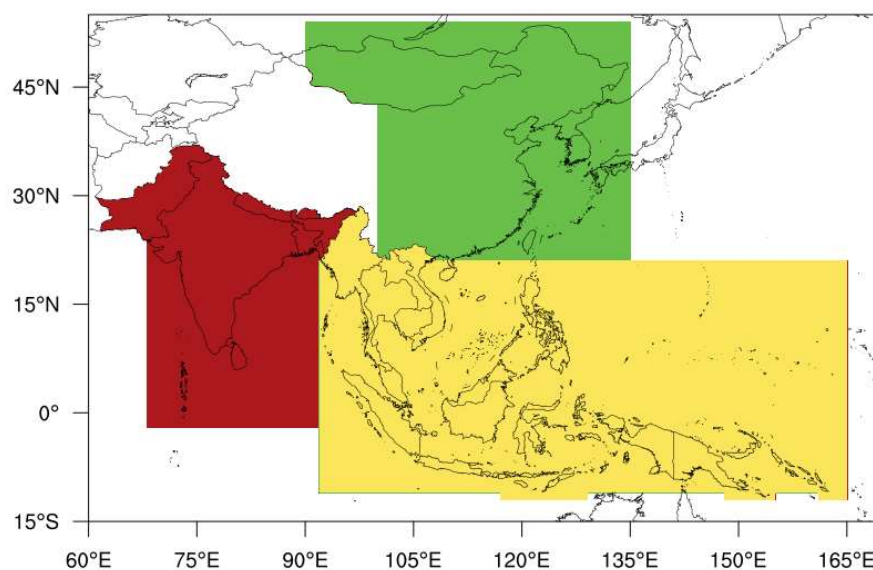


**Figure 2.** Division of the experimental area. The red shades represent South Asia. The green shades represent East Asia. The yellow shades represent Southeast Asia.

In this paper, five controlled experiments were conducted to simulate the atmospheric CO concentration in the summer from 2016–2020 (June, July and August) using the GEOS-Chem model.

UTLS high CO concentrations in the Asian monsoon region occurred over the Tibetan Plateau. To quantify the effect of surface emissions on CO concentrations in the UTLS over the Tibetan Plateau, a sensitivity experiment to simulate the distribution of CO atmospheric concentrations in 2016 was conducted to eliminate CO emissions in South Asia, East Asia and Southeast Asia. The effects of surface CO emissions in these regions on the global UTLS region were obtained by comparing three sensitivity experiments and control experiments. In these experiments, the effect of surface CO emissions on the CO concentration in the UTLS region could be obtained. The proportion of CO sources in the high-CO concentration region in the UTLS over the Tibetan Plateau could be quantified.

Chemical reactions are also an important way to generate CO. To quantify CO generated by chemical reactions, CH<sub>4</sub> and nonmethane VOCs (NMVOCs) worldwide were eliminated in the sensitivity experiment to simulate the atmospheric concentration distribution of CO in 2016. The effects of CH<sub>4</sub> and NMVOCs on CO concentrations in the UTLS region globally were obtained by analyzing the differences between the two sensitivity experiments and the 2016 control experiment.

## 2.2. Reanalysis Data

MERRA-2 is a reanalysis product issued by NASA that provides meteorological data documentation from 1 January 1980, to 31 January 2022. The assimilation system is an improvement over the original MERRA reanalysis data, enabling the assimilation of modern hyperspectral radiation and microwave observations, as well as GPS-radio datasets. Other advances in the GEOS model and GPS assimilation system are included in MERRA-2. The spatial resolution is roughly the same as that of MERRA. This article used MERRA-2 data downloaded from <http://geoschemdata.wustl.edu/>.

The Outgoing longwave radiation (OLR) generally refers to the long-wave radiation outward from the top of the atmosphere. The value of OLR is mainly determined by cloud and atmospheric temperature. The higher the cloud top, the lower the cloud top temperature, and the smaller the OLR. It means the stronger the convection. The low value region of the OLR is the main convective region. Convective systems can develop all the way up to the

tropopause. This paper uses the OLR global grid data the National Center for Atmospheric Research (NCAR)/National Centers for Environmental Prediction (NCEP)  $2.5^\circ \times 2.5^\circ$  in the summer of 2016 in the United States. This dataset can be downloaded at website: <https://climatedataguide.ucar.edu/climate-data/outgoing-longwave-radiation-olr-avhrr>, accessed on 15 May 2022. According to previous research [23],  $OLR \leq 220 \text{ W/m}^2$  was used in this paper to represent the region with a high incidence of deep convective activity.

### 2.3. Satellite Observation Data

The Microwave Limb Sounder (MLS) is an instrument aboard the sun-synchronous polar orbit satellite Aura. It can provide vertical profiles for various trace gases ( $\text{O}_3$ ,  $\text{CO}$ ,  $\text{N}_2\text{O}$  et al.) from the upper troposphere to the stratosphere. Compared to optical measurements, microwave detection is not affected by aerosols, cloud masks,  $\text{CO}_2$  or other factors in the atmosphere. The influence of the atmospheric temperature on meridional measurement and the measurement accuracy of the MLS is also limited. In this study, we used level 3 data of version 4.2 ([https://aura.gsfc.nasa.gov/mls\\_stratchem.html](https://aura.gsfc.nasa.gov/mls_stratchem.html), accessed on 15 May 2022). The spatial coverage is nearly global ( $82^\circ\text{N}$ – $82^\circ\text{S}$ ). The spatial resolution is  $4^\circ \times 5^\circ$  (latitude  $\times$  longitude) [24]. The recommended vertical range varies between 215 and 0.004 hPa. The vertical resolution is approximately 6 km.

## 3. Results

### 3.1. Model Evaluation

Figure 3 shows the five-year average (2016–2020) distribution characteristics of CO at 100 hPa and 215 hPa. The GEOS-Chem model simulation results and MLS satellite observations showed similar CO distribution characteristics at 100 hPa. In Figure 3a,b, there was only one high value region of the CO concentration located over the Tibetan Plateau in the Asian monsoon region. We interpolate the coordinate system of the model data into the coordinate system of the satellite data. The following calculation shall be carried out within the specified range:

$$A = \frac{G - M}{n}$$

$A$  is the average deviation of the two arrays.  $G$  represents the data of GEOS-Chem model.  $M$  stands for MLS satellite data and  $n$  represents the number of samples. In the latitude range of 100 hPa from  $45^\circ\text{S}$  to  $45^\circ\text{N}$ , at 100 hPa the average deviation between the simulated values and the satellite observations is 18.75 ppbv. The root mean square error of the two arrays is 19.82 ppbv and the correlation coefficient is 0.66. There were three high-value regions of the CO concentration at 215 hPa, which were distributed in North America, Asia and South Africa individually. Compared to Figure 3c,d, it could be found that the model suitably simulated the spatial distribution characteristics of these three high-value regions worldwide in the upper troposphere. In the upper troposphere, we compare the simulation results at 226 hPa to the 215 hPa satellite observations. In the latitude range of the upper troposphere from  $45^\circ\text{S}$  to  $45^\circ\text{N}$ , the average deviation between the simulated values and the satellite observations is 21.78 ppbv. The root mean square error of the two arrays is 13.10 ppbv and the correlation coefficient is 0.71. In UTLS the model simulates the distribution characteristics of CO, but underestimates the concentration of CO.

The GEOS-Chem model provides a more refined horizontal resolution grid and more accurate vertical resolution data than those associated with satellite observations. Based on these model characteristics, this study conveniently examined the process of CO transport from the ground to UTLS. In this paper, the GEOS-Chem model was used to simulate CO at the global UTLS height and explore the reasons for high-value regions over the Tibetan Plateau. In summary, the GEOS-Chem model could simulate the distribution characteristics of CO at the UTLS height in summer, and the deviations between the simulated and observed values could include uncertainties in the emission inventory used by the model, defects in the model and MLS, and errors in the reanalysis data such as the humidity.

Therefore, in the range of altitude and latitude bands considered in this paper, the GEOS-Chem model was used to study the transmission mechanism of the CO concentration high-value region at the UTLS height.

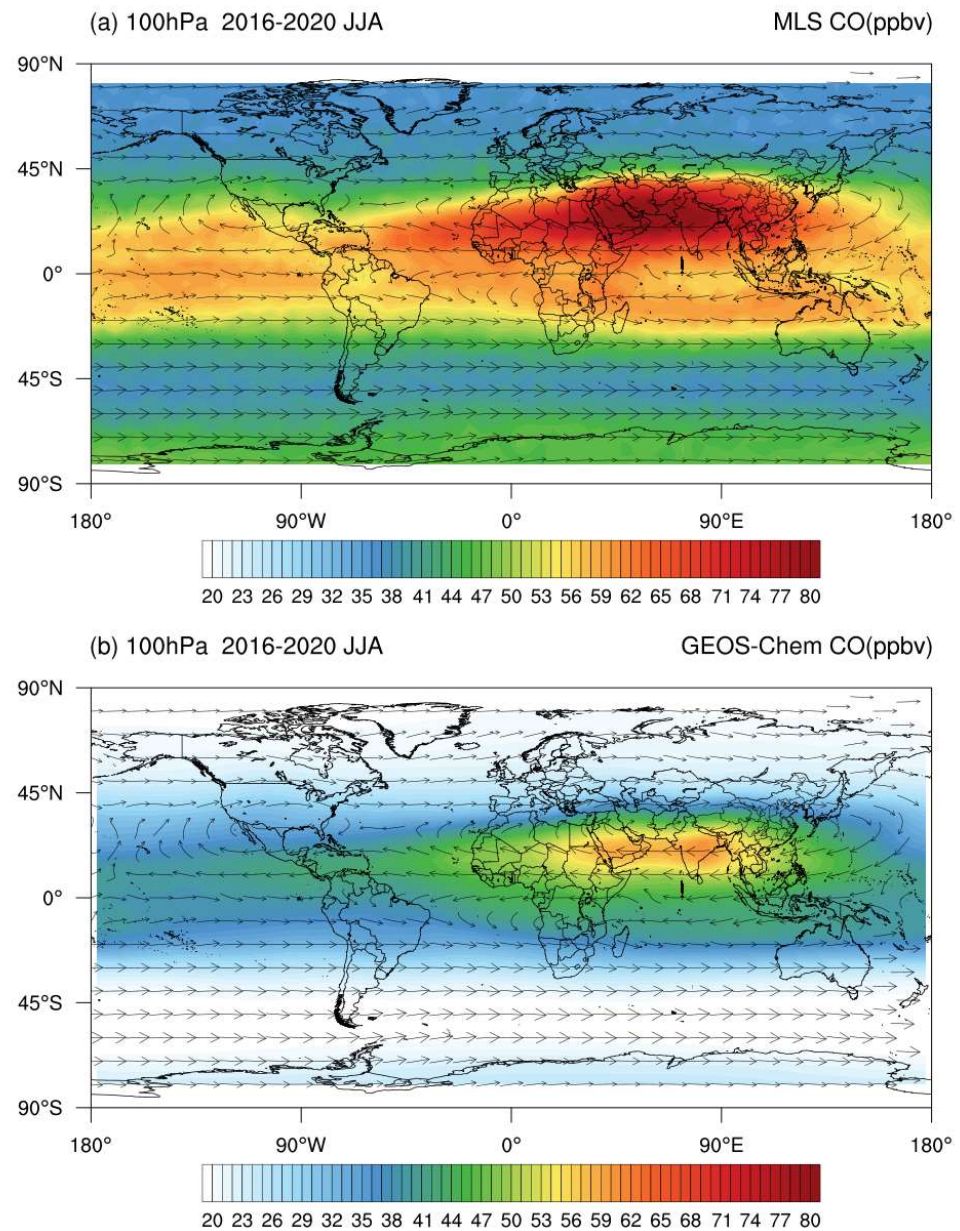
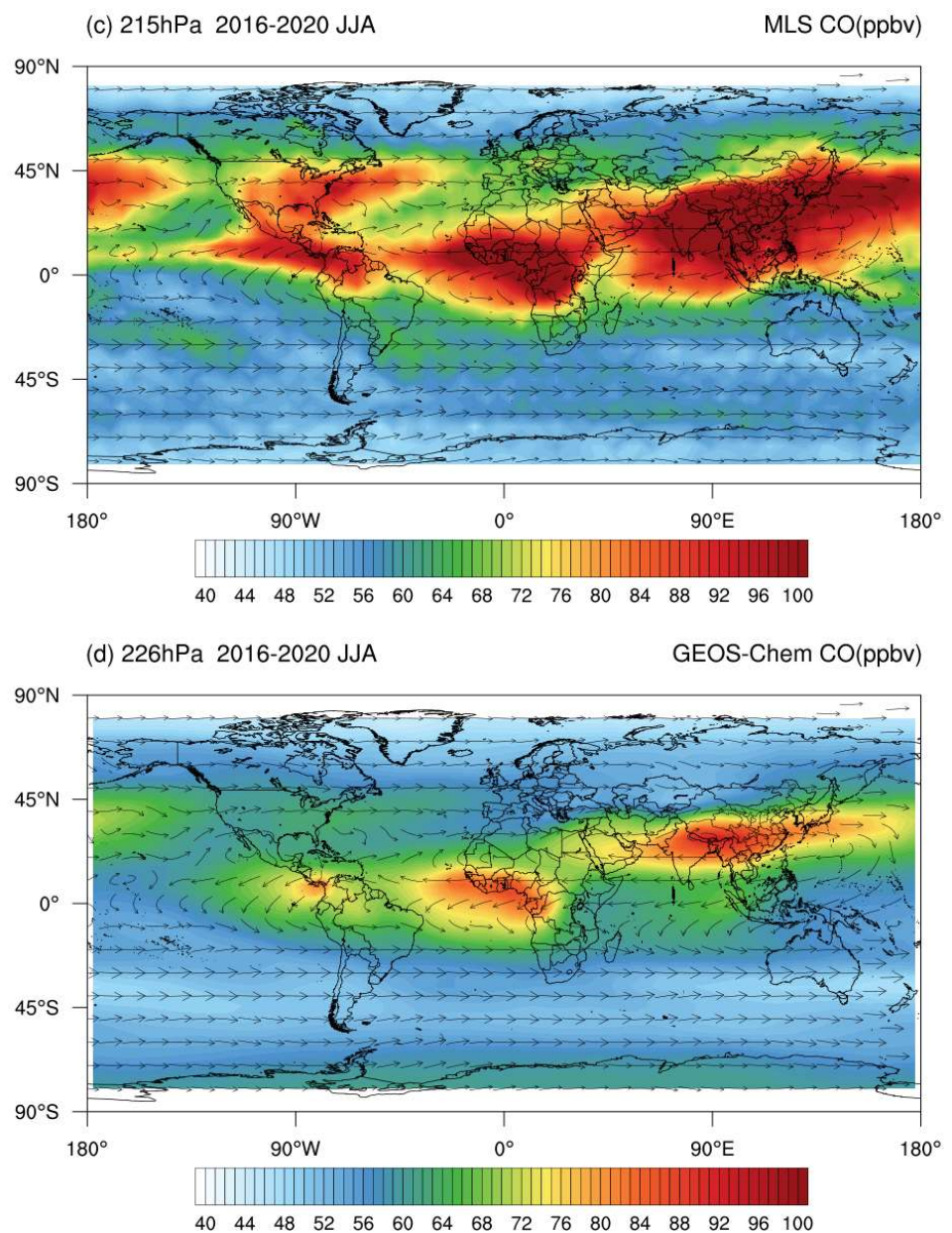


Figure 3. Cont.



**Figure 3.** Comparison of the observed CO values in the UTLS region to the simulated values. (a) MLS observation of the CO distribution at 100 hPa. (b) GEOS-Chem simulated CO distribution at 100 hPa. (c) MLS observation of the CO distribution at 215 hPa. (d) GEOS-Chem simulated CO distribution at 225 hPa. Units: ppbv. MERRA-2 reanalysis data are used for the wind field.

### 3.2. Transport of CO from the Surface to the UTLS

As shown in Figure 1, countries with high emissions, such as India and China, occur in the zone with a high incidence of deep convection activity. In addition, as shown in Figure 3c, the ASM anticyclone also corresponds to the position of a high incidence of deep convections. Air rich in CO with higher surface emissions is transported to the upper troposphere via deep convection. This air enters the ASM anticyclone in the upper troposphere. The strong ASM anticyclone obstructs the exchange of air inside and outside the anticyclone, forming a high-value area of the CO concentration. As shown in Figure 3a, the high-value centers of the CO concentration and the anticyclone center do not coincide. At 100 hPa, the intensity of the anticyclone is weakened, and the pollutants within the anticyclone flow from the southwest of the ASM anticyclone with atmospheric circulation.

### 3.3. Source of the CO High-Concentration Area at 100 hPa

To quantify the effects of surface emissions or atmospheric chemical reactions in different regions on the distribution of UTLS CO concentrations in summer, differences between the control and sensitivity tests were considered influences of regional emissions or precursor species. In this paper, two longitude regions were selected to represent the concentrations in the high-value CO region and nonhigh-value CO region. The difference in CO concentration between the high-value region (0–120°E) and nonhigh-value region (60–180°W) at the same latitude of 100 hPa was compared.

We set a mask in the target area, and CO emissions in the area covered by the mask will be automatically ignored in the calculation of the model. Figure 4 shows the effect of surface emissions on the 100 hPa CO concentrations in East Asia, South Asia and Southeast Asia. In the sensitivity experiment, we closed the regional emissions, and subtracted the results of the sensitivity experiment from the results of the control experiment to obtain the impact of regional emissions on the high-altitude CO concentration. At the top of each figure, the graphs give the average results for the latitudes with the highest concentrations of CO. We used 10–20°N mean results for East and Southeast Asia and the 20–30°N mean results for South Asia. The right side of the concentration diagram shows the difference between the high-value and nonhigh-value regions of CO at the different latitudes. In Figure 4a, only surface carbon monoxide emissions in South Asia are closed. Surface emissions in South Asia were mainly concentrated in the range from 20–30°N at 100 hPa, and the influence on the CO concentration reached up to 14 ppbv. Combined with an analysis of the circulation field, surface CO in South Asia was transported to 100 hPa by the deep convection system and diffused westward with monsoon circulation. In Figure 4b, only surface CO emissions in East Asia are closed. The distribution characteristics of CO emissions originating from East Asia and South Asia at the 100 hPa height were similar, concentrated over the Asian monsoon region, and gradually weakened near the Tibetan Plateau. Compared to the other two regions, the emissions in Southeast Asia yielded a wider impact, including on the CO concentration in the Asian monsoon region. In Figure 4c, only surface CO emissions in Southeast Asia are closed. The CO emissions stemming from Southeast Asia accumulated in the range from 10–20°N at 100 hPa. The maximum influence on the atmospheric CO concentration at 100 hPa was 2.67 ppbv. This was the region with the smallest influence on the 100 hPa CO concentration among the three regions selected in this chapter.

We shut down the global flux of CO chemically reactive species from the ground to the stratosphere. The effect of species on CO concentrations in the UTLS can obtain using the results of the control experiments minus the results of the experiments that shut down the global flux. Figure 5 shows the effects of CO, CH<sub>4</sub> and NMVOC emissions on the concentration in the high-value region at 100 hPa. In the global UTLS region, CH<sub>4</sub> generated a greater influence on CO concentrations than that of NMVOCs. In the lower stratosphere, both CH<sub>4</sub> and CO generated by NMVOCs exhibited the characteristics of a high-CO value region over the Tibetan Plateau. The global surface CO emissions at 100 hPa were concentrated in the Asian monsoon region, while the maximum values reached 22.47 ppbv.

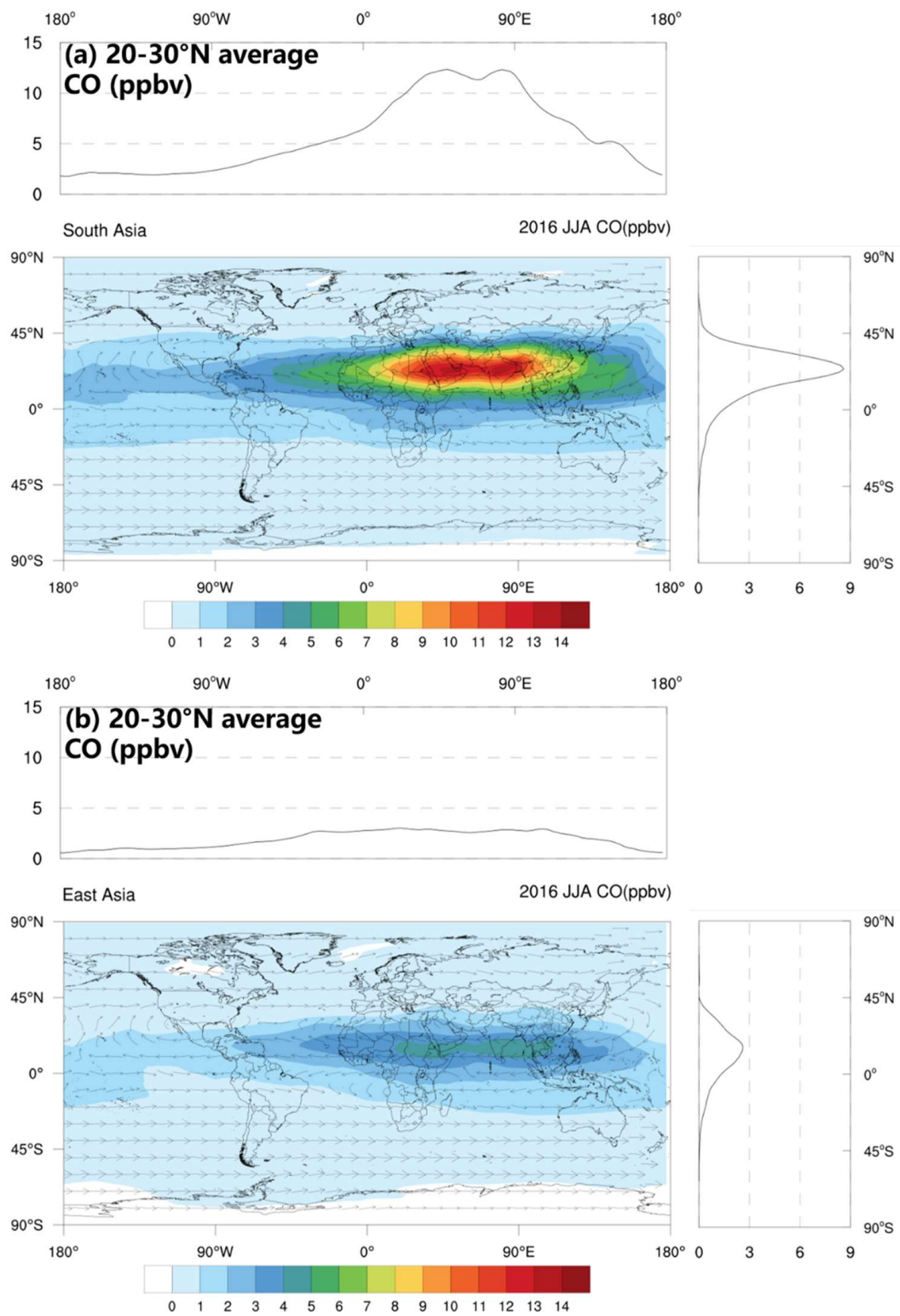
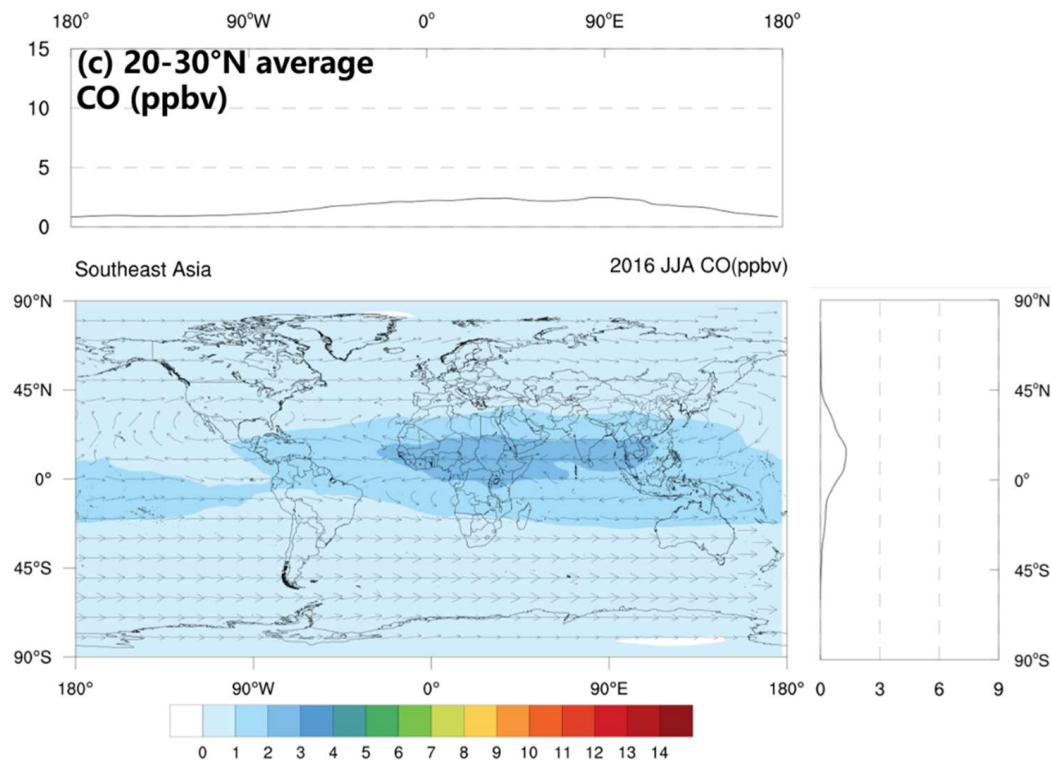


Figure 4. Cont.



**Figure 4.** Effect of surface emissions on the 100 hPa CO concentrations in South Asia (a), East Asia (b) and Southeast Asia (c). At the top of the concentration graph are the average results for the latitudes with the highest concentrations of CO. The right side of the concentration diagram shows the difference between the high-value and nonhigh-value regions of CO at the different latitudes. Units: ppbv.

As indicated in Table 1, the simulation results of the GEOS-Chem model were lower than the MLS satellite observations. The underline indicates the maximum impact of the species or region on CO concentration at different latitudes. However, from 10–60°N, the data showed similar characteristics. The CO concentration was concentrated from 0–40°N. Concentrations were higher in the Northern Hemisphere than those in the Southern Hemisphere. Regarding the difference in CO concentration between the inside and outside of the anticyclone at 100 hPa, 43.18% originated from CH<sub>4</sub> chemical reactions, NMVOC chemical reactions accounted for 20.81%, surface CO emissions accounted for 63.33%, and the effect of sinks reached –27.32%. Regarding surface CO emissions, East Asia contributed 13.56%, South Asia contributed 39.27%, and Southeast Asia contributed 7.15%.

**Table 1.** Differences in the CO concentration in two longitude ranges. Units: ppbv.

Latitude (°N)	East Asia	South Asia	Southeast Asia	CO Emissions	CH <sub>4</sub>	NMVOCs	Control Experiment	MLS
–10–0	0.87	0.92	0.52	2.90	3.05	1.33	6.20	2.24
0–10	1.77	2.10	1.08	4.71	3.97	1.50	8.49	3.24
10–20	<u>2.51</u>	4.68	<u>1.27</u>	8.73	6.21	2.81	14.41	14.67
20–30	1.84	<u>8.18</u>	0.86	<u>11.86</u>	<u>7.19</u>	<u>3.90</u>	<u>17.95</u>	<u>21.88</u>
30–40	0.84	4.99	0.45	6.90	4.56	2.36	10.08	13.74
40–50	0.07	0.96	0.08	1.25	0.99	0.44	1.82	3.32
50–60	0.01	0.16	0.03	0.24	0.25	0.13	0.60	0.47

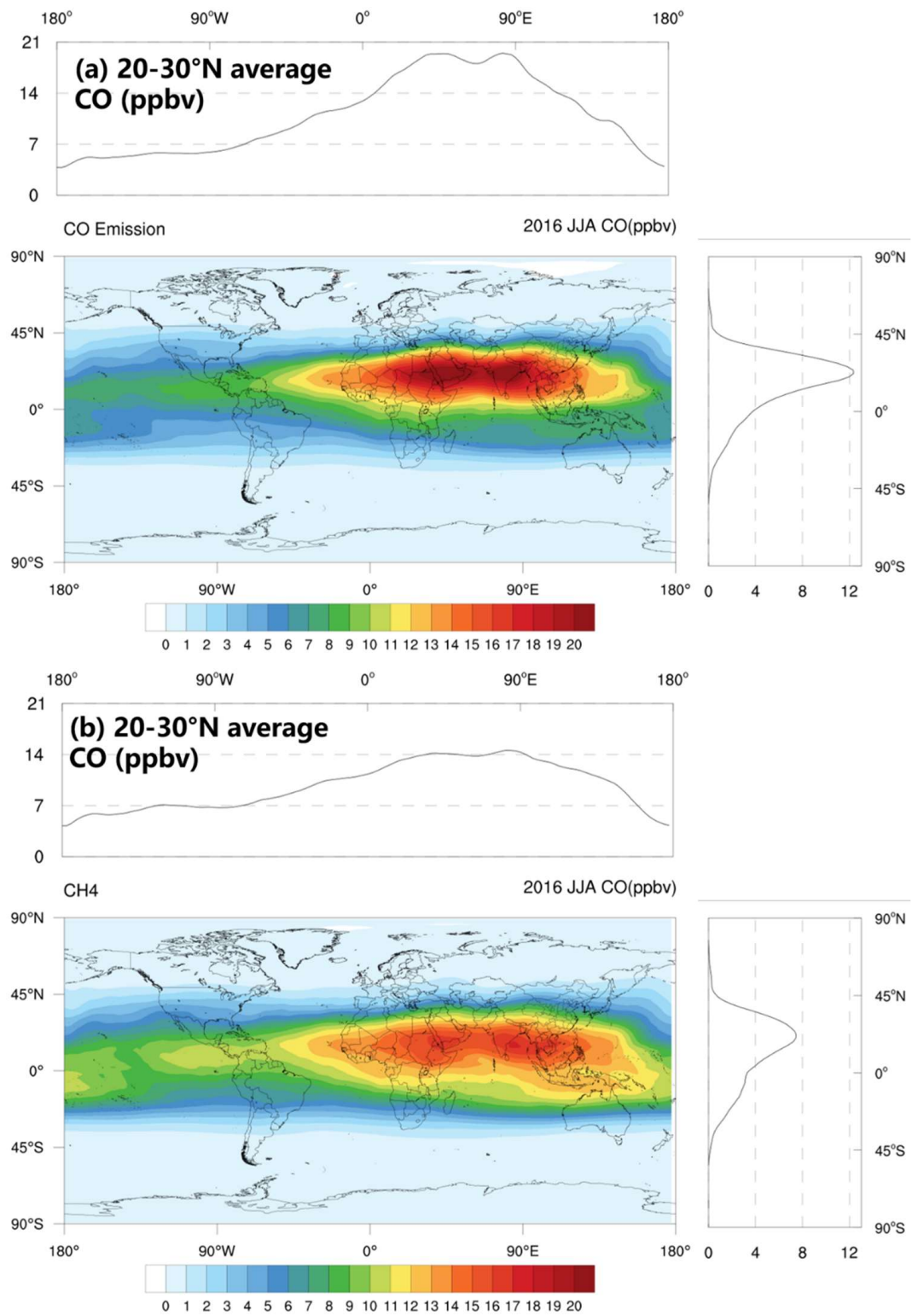
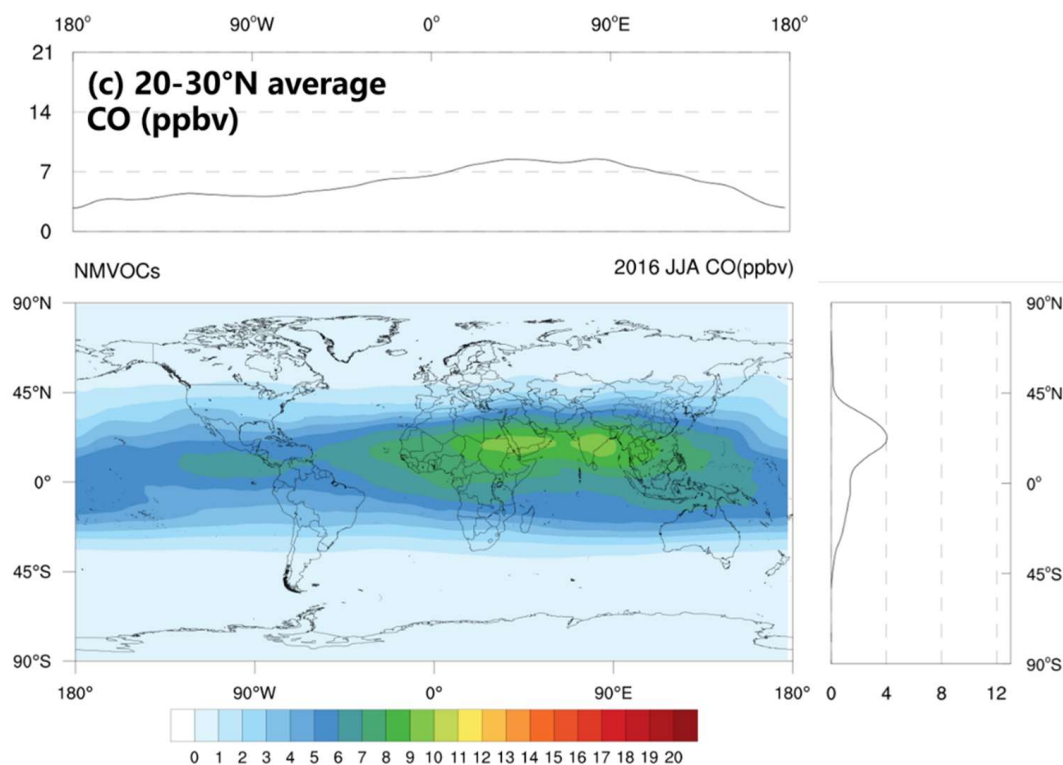


Figure 5. Cont.



**Figure 5.** Effects of CO emissions (a) CH<sub>4</sub> (b) and NMVOCs (c) on CO concentration in the UTLS.

#### 4. Conclusions

In this paper, we used the GEOS-Chem chemical transport model and MLS satellite observation data to analyze the origin of CO concentration high-value regions in the UTLS over the Tibetan Plateau. The effects of CO and chemical reaction species emissions on UTLS high CO concentrations were investigated using numerical models. Combined with the satellite observation results of the MLS, the formation mechanism of the high-value region of CO over the Tibetan Plateau and the transport path and transport mechanism of CO from surface emissions to the upper troposphere and lower stratosphere were explored.

The GEOS-Chem model accurately simulated the CO concentration in the UTLS. The CO emissions stemming from the surface of the Asian monsoon region were transported via deep convections to the upper troposphere and lower stratosphere within the ASM anticyclone. The ASM anticyclone prevented air exchange between the inside and the outside of the anticyclone and helped to form a high-CO concentration area in the UTLS region. According to the model simulation results, the CO concentration at 100 hPa in the Asian monsoon region was higher than that in the other regions at the same latitude. Regarding effects, 43.18% originated from CH<sub>4</sub> chemical reactions, 20.81% originated from NMVOC chemical reactions, and 63.33% originated from surface CO emissions, while sinks yielded a negative contribution of −27.32%. Surface CO emissions were the main reason for this difference. CH<sub>4</sub> imposed a greater effect on the CO concentration than that of NMVOCs at 100 hPa. Regarding surface CO emissions, East Asia contributed 13.56%, South Asia contributed 39.27%, and Southeast Asia contributed 7.15%.

**Author Contributions:** Conceptualization, Q.L.; Data curation, Y.Y.; Formal analysis, H.W. and W.W.; Investigation, H.W. and Z.B.; Resources, H.W. and D.L.; Validation, Q.L.; Visualization, Y.Y.; Writing—original draft, Y.Y.; Writing—review & editing, Q.L. and J.B. All authors have read and agreed to the published version of the manuscript.

**Funding:** This work was supported by the strategic priority research program of the Chinese Academy of Sciences (Grant No. XDA17010102), the second Tibetan Plateau Scientific Expedition and Research Program (STEP, 2019QZKK0604), the National Natural Science Foundation of China (Grant Nos. 91637104, 91837311, and 42061134012), and the National Key Research and Development Program of China (Grant No. 2018YFC1505703).

**Acknowledgments:** This work used the GEOS-Chem model. Central management and support of the model were provided by the Atmospheric Chemistry Modeling Group at Harvard University and by the Atmospheric Composition Analysis Group at Washington University. We thank the NCAR for the OLR data and NASA MLS satellite data.

**Conflicts of Interest:** The authors declare no conflict of interest.

## References

1. Mohanakumar, K. Stratospheric ozone depletion and Antarctic ozone hole. In *Stratosphere Troposphere Interactions: An Introduction*; Springer: Dordrecht, The Netherlands, 2008; pp. 253–305.
2. Brewer, A. Evidence for a world circulation provided by the measurements of helium and water vapour distribution in the Stratosphere. *Q. J. R. Meteorol. Soc.* **1949**, *75*, 351–363. [[CrossRef](#)]
3. Dobson, G.M.B. Origin and distribution of the polyatomic molecules in the atmosphere. *Proc. R. Soc. London. Ser. A Math. Phys. Sci.* **1956**, *236*, 187–193.
4. Birner, T. Fine-scale structure of the extratropical Tropopause region. *J. Geophys. Res. Atmos.* **2006**, *111*, D04104. [[CrossRef](#)]
5. Mote, P.W.; Rosenlof, K.H.; McIntyre, M.E.; Carr, E.S.; Gille, J.C.; Holton, J.R.; Kinnerson, J.S.; Pumphrey, H.C.; Russell, J.M., III; Waters, J.W. An atmospheric tape recorder: The imprint of tropical Tropopause temperatures on Stratospheric water vapor. *J. Geophys. Res. Atmos.* **1996**, *101*, 3989–4006. [[CrossRef](#)]
6. Ninomiya, K.; Shibagaki, Y. Cloud system families in the Meiyu-Baiu front observed during 1–10 July 1991. *J. Meteorol. Soc. Japan. Ser. II* **2003**, *81*, 193–209. [[CrossRef](#)]
7. Randel, W.J.; Park, M.; Emmons, L.; Kinnison, D.; Bernath, P.; Walker, K.A.; Boone, C.; Pumphrey, H. Asian monsoon transport of pollution to the Stratosphere. *Science* **2010**, *328*, 611–613. [[CrossRef](#)]
8. Bian, J.; Pan, L.L.; Paulik, L.; Vömel, H.; Chen, H.; Lu, D. In situ water vapor and ozone measurements in Lhasa and Kunming during the Asian summer monsoon. *Geophys. Res. Lett.* **2012**, *39*, L19808. [[CrossRef](#)]
9. Yu, P.; Rosenlof, K.H.; Liu, S.; Telg, H.; Thornberry, T.D.; Rollins, A.W.; Portmann, R.W.; Bai, Z.; Ray, E.A.; Duan, Y.; et al. Efficient transport of tropospheric aerosol into the stratosphere via the Asian summer monsoon anticyclone. *Proc. Natl. Acad. Sci. USA* **2017**, *114*, 6972–6977. [[CrossRef](#)]
10. Park, M.; Randel, W.J.; Kinnison, D.E.; Garcia, R.R.; Choi, W. Seasonal variation of methane, water vapor, and nitrogen oxides near the Tropopause: Satellite observations and model simulations. *J. Geophys. Res. Atmos.* **2004**, *109*, D03302. [[CrossRef](#)]
11. Li, Q.; Jiang, J.H.; Wu, D.L.; Read, W.G.; Livesey, N.J.; Waters, J.W.; Zhang, Y.; Wang, B.; Filipiak, M.J.; Davis, C.P. Trapping of Asian pollution by the Tibetan anticyclone: A global CTM simulation compared with EOS MLS observations. *Geophys. Res. Lett.* **2005**, *32*, L14826. [[CrossRef](#)]
12. Dessler, A.E. A determination of the cloud feedback from climate variations over the past decade. *Science* **2010**, *330*, 1523–1527. [[CrossRef](#)] [[PubMed](#)]
13. Ehhalt, D.; Rohrer, F.; Wahner, A.; Prather, M.; Blake, D. On the use of hydrocarbons for the determination of Tropospheric OH concentrations. *J. Geophys. Res. Atmos.* **1998**, *103*, 18981–18997. [[CrossRef](#)]
14. Park, M.; Randel, W.J.; Gettelman, A.; Massie, S.T.; Jiang, J.H. Transport above the Asian summer monsoon anticyclone inferred from Aura Microwave Limb Sounder tracers. *J. Geophys. Res. Atmos.* **2007**, *112*, D16309. [[CrossRef](#)]
15. Park, M.; Randel, W.J.; Emmons, L.K.; Livesey, N.J. Transport pathways of carbon monoxide in the Asian summer monsoon diagnosed from Model of Ozone and Related Tracers (MOZART). *J. Geophys. Res. Atmos.* **2009**, *114*, D08303. [[CrossRef](#)]
16. Duncan, B.N.; Martin, R.V.; Staudt, A.C.; Yevich, R.; Logan, J.A. Interannual and seasonal variability of biomass burning emissions constrained by satellite observations. *J. Geophys. Res. Atmos.* **2003**, *108*, ACH 1-1–ACH 1-22. [[CrossRef](#)]
17. Zhao, C.; Peng, L.; Tie, X.; Lin, Y.; Li, C.; Zheng, X.; Fang, Y. A high CO episode of long-range transport detected by MOPITT. *Water Air Soil Pollut.* **2007**, *178*, 207–216. [[CrossRef](#)]
18. Luo, J.; Tian, W.; Pu, Z.; Zhang, P.; Shang, L.; Zhang, M.; Hu, J. Characteristics of Stratosphere-Troposphere exchange during the Meiyu season. *J. Geophys. Res. Atmos.* **2013**, *118*, 2058–2072. [[CrossRef](#)]
19. Marais, E.A.; Wiedinmyer, C. Air quality impact of diffuse and inefficient combustion emissions in Africa (DICE-Africa). *Environ. Sci. Technol.* **2016**, *50*, 10739–10745. [[CrossRef](#)]

20. Li, M.; Zhang, Q.; Kurokawa, J.-i.; Woo, J.-H.; He, K.; Lu, Z.; Ohara, T.; Song, Y.; Streets, D.G.; Carmichael, G.R. MIX: A mosaic Asian anthropogenic emission inventory under the international collaboration framework of the MICS-Asia and HTAP. *Atmos. Chem. Phys.* **2017**, *17*, 935–963. [[CrossRef](#)]
21. Wiedinmyer, C.; Yokelson, R.J.; Gullett, B.K. Global emissions of trace gases, particulate matter, and hazardous air pollutants from open burning of domestic waste. *Environ. Sci. Technol.* **2014**, *48*, 9523–9530. [[CrossRef](#)]
22. Guenther, A.; Karl, T.; Harley, P.; Wiedinmyer, C.; Palmer, P.I.; Geron, C. Estimates of global terrestrial isoprene emissions using MEGAN (Model of Emissions of Gases and Aerosols from Nature). *Atmos. Chem. Phys.* **2006**, *6*, 3181–3210. [[CrossRef](#)]
23. Camara, M.; Diedhiou, A.; Gaye, A. African easterly waves and cyclonic activity over the eastern Atlantic: Composite and case studies. *Int. J. Geophys.* **2011**, *2011*, 874292. [[CrossRef](#)]
24. Schwartz, M.; Pumphrey, H.; Livesey, N.; Read, W.; Fuller, R. *MLS/Aura Level 3 Monthly Binned Carbon Monoxide (CO) Mixing Ratio on Assorted Grids V005*; Goddard Earth Sciences Data and Information Services Center (GES DISC): Greenbelt, MD, USA, 2021. [[CrossRef](#)]